1

Virgo Data Analysis for C6 and C7 engineering runs

F. Acernese[6], P. Amico[10], M. Alshourbagy[11], F. Antonucci [12], S. Aoudia[7], P. Astone[12], S. Avino[6], D. Babusci[4], G. Ballardin[2], F. Barone[6], L. Barsotti[11], M. Barsuglia[8] , F. Beauville[1], S. Bigotta[11], S. Birindelli[11], M.A. Bizouard[8], C. Boccara[9], F. Bondu[7], L. Bosi[10], C. Bradaschia[11], S. Braccini[11],A. Brillet[7], V. Brisson[8], L. Brocco[12], D. Buskulic[1], E. Calloni[6], E. Campagna[3], F. Carbognani[2], F. Cavalier[8], R. Cavalieri[2], G. Cella[11], E. Cesarini[3], E. Chassande-Mottin[7], N. Christensen[2], C. Corda[11], A. Corsi[12], F. Cottone[10], A.-C. Clapson[8], F. Cleva[7], J.-P. Coulon[7], E. Cuoco[2], A. Dari[10], V. Dattilo[2], M. Davier[8], M. del Prete[2], R. De Rosa[6], L. Di Fiore[6], A. Di Virgilio[11], B. Dujardin[7], A. Eleuteri[6], I. Ferrante[11], F. Fidecaro[11], I. Fiori[11], R. Flaminio[1], 2, J.-D. Fournier[7], O.Francois[2], S. Frasca[12], F. Frasconi[2,11], L. Gammaitoni[10], F. Garufi[6], E. Genin[2], A. Gennai[11], A. Giazotto[11], G. Giordano[4], L. Giordano[6], R. Gouaty[1], D. Grosjean[1], G. Guidi[3], S. Hebri[2], H. Heitmann[7], P. Hello[8], S. Karkar[1], S. Kreckelbergh[8], P. La Penna[2], M. Laval[7], N. Leroy[8], N. Letendre[1], B. Lopez[2], Lorenzini[3], V. Loriette[9], G. Losurdo[3], J.-M. Mackowski[5], E. Majorana[12], C. N. Man[7], M. Mantovani[11], F. Marchesoni[10], F. Marion[1], J. Marque[2], F. Martelli[3], A. Masserot[1], M. Mazzoni[3], L. Milano[6], F. Menzinger[2], C. Moins[2], J. Moreau[9], N. Morgado[5], B. Mours[1], F. Nocera[2], A. Pai[12], C. Palomba[12], F. Paoletti[2], 11, S. Pardi[6], A. Pasqualetti[2], R. Passaquieti[11], D. Passuello[11], B. Perniola[3], F. Piergiovanni[3], L. Pinard[5], R. Poggiani[11], M. Punturo[10], P. Puppo[12], K. Qipiani[6], P. Rapagnani[12], V. Reita[9], A. Remillieux[5], F. Ricci[12], I. Ricciardi[6], P. Ruggi [2], G. Russo[6], S. Solimeno[6], A. Spallicci[7], R. Stanga[3], T. Marco[11], M. Tonelli[11], A. Toncelli[11], E. Tournefier[1], F. Travasso[10], C. Tremola[11], G. Vajente [11], D. Verkindt[1], F. Vetrano[3], A. Viceré[3], J.-Y. Vinet[7], H. Vocca[10] and M. Yvert[1]

[1]*Laboratoire d'Annecy-le-Vieux de Physique des Particules (LAPP), IN2P3/CNRS, Université de Savoie, Annecy-le-Vieux, France;*

[2]*European Gravitational Observatory (EGO), Cascina (Pi), Italia;*

[3]*INFN, Sezione di Firenze/Urbino, Sesto Fiorentino, and/or Università di Firenze, and/or Università di Urbino, Italia;*

[4]*INFN, Laboratori Nazionali di Frascati, Frascati (Rm), Italia;*

[5]*LMA, Villeurbanne, Lyon, France;*

[6]*INFN, sezione di Napoli and/or Università di Napoli "Federico II" Complesso Universitario di Monte S.Angelo, and/or Università di Salerno, Fisciano (Sa), Italia;*

[7]*Departement Artemis – Observatoire de la Côte d'Azur, BP 42209 06304 Nice, Cedex 4,*

2

France;

[8]*Laboratoire de l'Accélérateur Linéaire (LAL), IN2P3/CNRS Université de Paris-Sud, Orsay,*
France;

[9]*ESPCI, Paris, France;*

[10]*INFN, Sezione di Perugia and/or Università di Perugia, Perugia, Italia;*

[11]*INFN, Sezione di Pisa and/or Università di Pisa, Pisa, Italia;*

[12]*INFN, Sezione di Roma and/or Università "La Sapienza", Roma, Italia.*

The interferometric gravitational wave detector Virgo its completing the commissioning phase, and it is close to commencing with scientific data taking. In 2005, before a temporary shutdown of the interferometer, two commissioning runs were performed: the C6 run from July 29th to August 12th, and the C7 run from September 14th to 19th. The sensitivity of the detector during these commissioning runs was not yet at an interesting level for scientific observations. However, the bandwidth and stability of the detector is already sufficient to perform important studies in preparation for the acquisition and analysis of astrophysically important data. The data have therefore been analyzed by the Virgo physics groups, with the goal of testing the analysis pipelines and developing veto strategies. The results also allowed a better understanding of the noise sources, thus providing useful feedback to the commissioning team.

1. Introduction

The interferometric gravitational wave (GW) detector Virgo is completing the preliminary phase of commissioning before commencing with the collection of data of astrophysical interest. During 2005, two commissioning runs were performed, the C6 run from July 29th to August 12th and the C7 run from September 14th to 19th. The best sensitivity attained was not yet useful for astrophysical observations. However, the detector performance was characterized by a high duty cycle and a sufficient stability for collecting long stretches of data. This was extremely useful for the noise characterization of the detector, to define the veto procedures, and for assessing the causes limiting the actual sensitivity. In this analysis effort we took advantage of on-line tools that permit one to monitor some of the noise features of the detector, such as changes in specific *spectral* lines and the long-term stationarity of the background noise.

The collected data have also been analyzed so as to test our search strategies for GW signals embedded in the detector noise. In particular we focused our attention on those periods of time in the runs during which we inserted, via hardware injections, signals into the VIRGO interferometer, thereby simulating the effects of a GW from a coalescing binary system or a supernova.

In the first section of this paper we summarize the general features of the data collected during the C6 and C7 runs. In section 3 we report on the analysis concerning the noise characterization of the detector. In section 4 we described the hardware injections of simulated GW signals. In section 5 and 6 we discuss the

analysis results from searching for transient gravitational wave signals. In section 7 we report on the GW stochastic background search based on the cross correlation of data collected by VIRGO and the bar detectors AURIGA, EXPLORER and NAUTILUS. The analysis method and the results on the C6 and C7 data for the continuous GW signals are reported in a separate article of these proceedings [28].
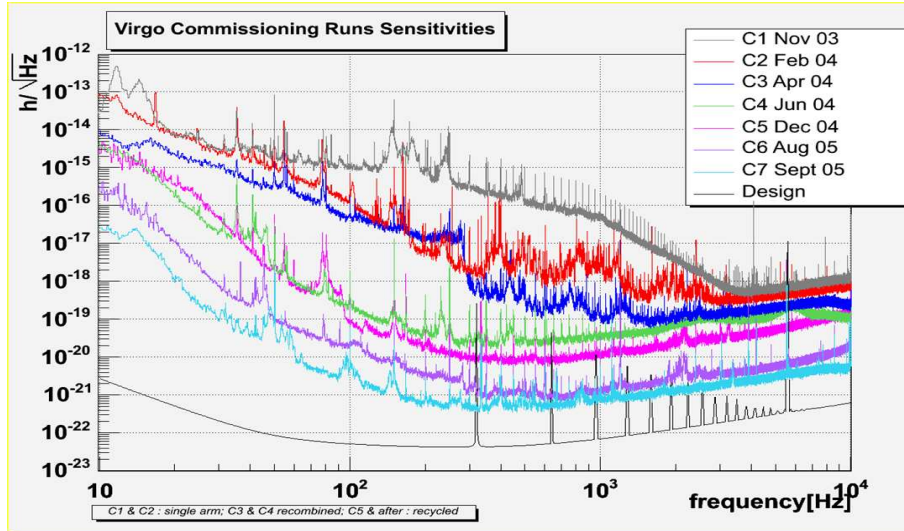
2. C6-C7 run description

Fig. 1.   The Virgo noise sensitivity curves for the commissioning runs C1 through C7. The bottom line represents the Virgo design sensitivity (assuming 10 W of laser power).

In the 2005 two main commissioning runs were performed, C6 and C7. Fig. 1 displays the Virgo sensitivity for all of our commissioning runs to date. The C6 run lasted 14 days with a duty cycle in science mode of 85%.
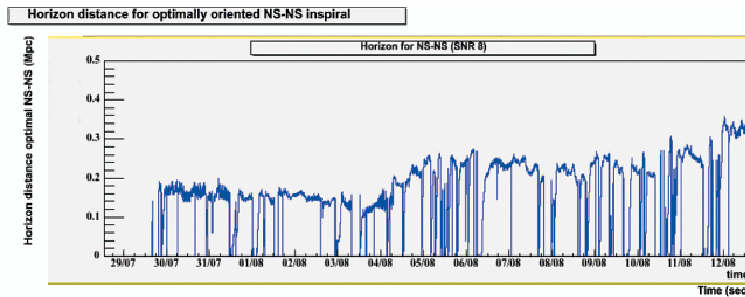

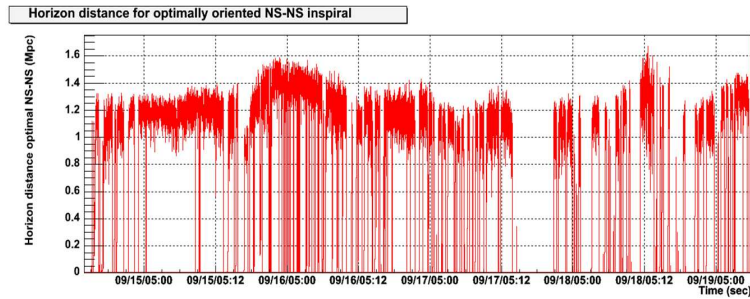Fig. 2.   The C6 binary neutron star horizon distance

4

Fig. 3.   The C7 binary neutron star horizon distance.

In Fig. 2 we show the time evolution of the detector sensitivity expressed in terms of the distance from the Earth of a binary coalescence event (*horizon distance*), i.e. the distance for the detection of a coalescing binary system of two 1.4 $M_\odot$ neutron stars, optimally oriented with respect to VIRGO and with a signal to noise ratio (SNR) of 8. The C7 run was performed in September 2005 and spanned 5 days, with a duty cycle of 65%; Fig. 3 displays the C7 horizon distance.

3. Detector characterization

The data collected in both runs were analyzed by the noise group with the aim of fully characterizing the main features of the noise distribution. In particular we tried to identify all the spectral lines of our sensitivity curve, calculating the coherence with a number of interferometer auxiliary and environmental channels [25]. All the identified lines were cataloged and sent to a database. Fig. 4 displays a snapshot of how our lines database looks like.

We investigated also the stationarity of the noise, looking at the slow non stationarity and at the transient-like signals. For example, we identified the source of non stationary noise, found just after the locking of the interferometer. Analyzing the data, after a whitening procedure, we identified the source of noise as due to the ring-down effect of some modes of our mirrors or their suspending wires, either violin modes or drum modes. In the left plot of Fig. 5 we show the SNR of the events detected by one of our transient search algorithms (WDF [2]) with respect to time just after locking. In it evident that just after the lock acquisition the event rate and the SNR is very high. The right plot of Fig. 5 shows the spectrogram of the dark fringe whitened channel where the excited lines just after the locking of the interferometer are clearly visible. These excited lines were identified as due to violins and mirrors drum modes ring-down [25].

Moreover we tried to identify the main sources for transient-like events. As reported in the following section, this work is fundamental for the burst detection analysis, where we have to clearly separate noise events from potential GW signals. We run burst detection algorithms on the data from the interferometer's dark fringe

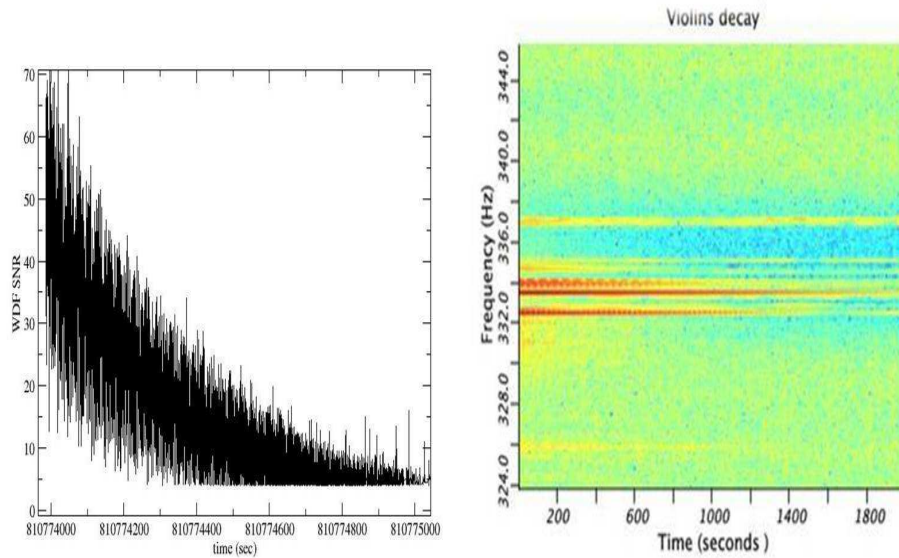Fig. 4.   A snapshot of the Virgo database for lines

Fig. 5.   Ring-down effect after lock acquisition, seen by an external trigger generator. In the first left are the events found by the WDF algorithm, while in the right plot displays the spectrogram of the whitened dark fringe signal, just after locking, in the band of $300-330$ Hz. The violin modes of mirror suspension wires are clearly excited.

channel and on a set of other interferometer and environmental channels. In Fig. 6 we show two examples of transient-like events identified in a magnetometer sensor

6

and another in a seismometer. The first is due to a lighting, the second to an an airplane flying close to the building of Virgo.
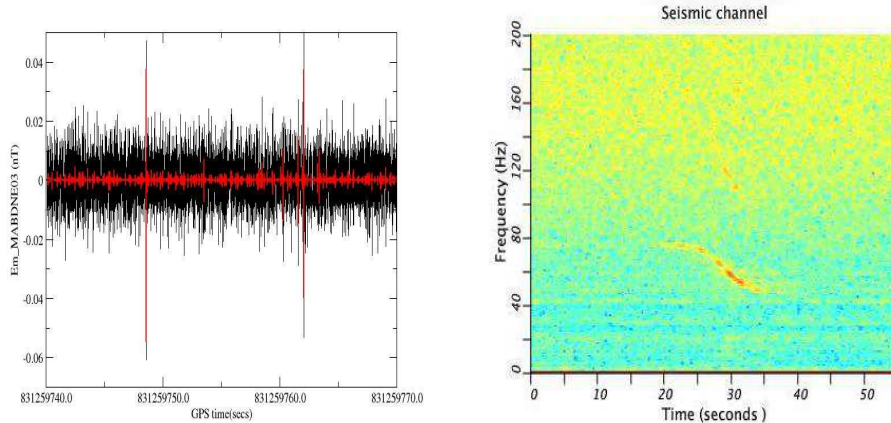

Fig. 6.   Example of lightening event on a magnetometer channel (left) in the time-domain plot and the effect of an airplane flying close to Virgo, seen by a seismometer channel (right). In the time frequency plot of the whitened data are evident the chirp of the noise and its harmonics.

4. Hardware injections of Gravitational Wave signals

Hardware injections are performed routinely in Virgo to cross-check the control, reconstruction and analysis pipeline, and to allow testing for the safety of the veto procedures. The injections are performed by inducing a variation in the length of the North arm Fabry-Perot cavity, by means of an appropriate force time-series applied to the cavity input mirror. As such, the signals influence not only the differential signal, but also the common mode, and can be regarded as corresponding to the effect of a waveform propagating along the West axis of the interferometer. The force time-series is computed assuming that the response of the mirror to external forces is the one of a simple pendulum; this is very accurate well below the internal resonances of the mirror, specifically below 5 kHz. Under these assumptions, the relation between the force F and the GW signal h is simply

$$F(\omega) = MLh(\omega)(\omega_0^2 - \omega^2) \tag{1}$$

where M is the mirror mass (21.3 kg), $L = 3000$m is the cavity length, and $\omega_0 = 2\pi 0.6$ Hz is the resonant frequency of the mirror pendulum. This relation is used, in the time domain, to convert a given impulsive signal into a force time series. This force time-series is further converted into a voltage, applied to the coils acting on the mirror magnets, compensating for the current-voltage characteristic. The injection time series are sampled at 10 kHz, which is more than adequate for signals

with frequency content safely below 5 kHz. The North input mirror is not controlled along the longitudinal degree of freedom, and therefore the only signals sent to this mirror are hardware injections. This is very important, since the h-reconstruction procedure makes use of the control signals, and partially cancels their effect in the h-stream. But since the North input mirror is left free, its control signal is not used, and consequently the injected GW signal is left unaffected. During C6, hardware injections were performed every four days, with only two kind of waveforms: binary neutron star signals, with 1.4 - 1.4 $M_\odot$, starting at 50Hz, and sine-gaussian signals with central frequency of 460Hz and quality factor Q=15. Binary neutron star signals were injected over a period of an hour during each injection session, with an average interval of 4 minutes between individual injections. The sine-gaussian signals were injected over an hour at each session, with an average interval of 1 minute. During C7, other impulsive waveforms were added: sine-gaussian signals with central frequency 920 Hz, and gaussian signals with width of 2 ms. To accommodate the greater variety of signals, the injection rate of bursts during an injection session was one every 20 s during C7. During both runs, the intended SNR of the injections was 15 for the bursts, and 20 for the binary neutron star events. The actual SNR varied from one injection session to another, according to the actual noise level.
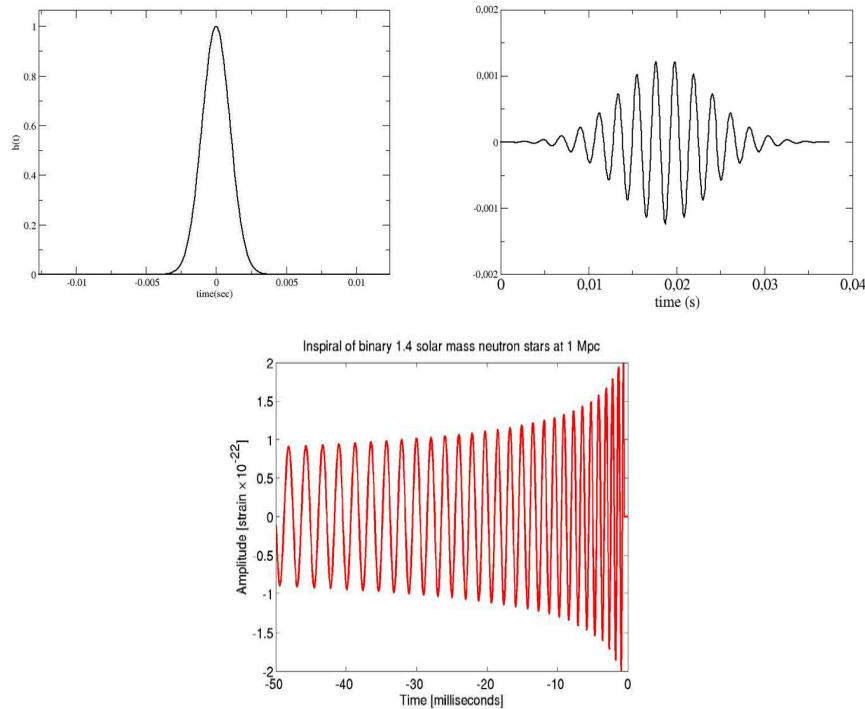
8

Fig. 7.   Gravitational wave signal waveforms for the injected signals: on top are two burst-like signals, gaussian (left) and sine-gaussian (right). On the bottom, a coalescing binaries signal.

5. Burst analysis

The detection of GW bursts emitted by star collapse or super-novae is one of the most difficult tasks for the GW community due to the fact that there are uncertainties in the exact shape of the waveforms, as we do not have complete models. A major task for this kind of detection effort is the cleaning of the event triggers found by the detection pipelines, namely the removal of accidental transient signals due to noise source events. The burst analysis for C6/C7 run was mainly an analysis devoted to the understanding of the machine and to the identification of the big transient events we found in our data.

5.1. *Virgo burst pipelines*

The Virgo burst search group uses a number of different techniques in order to find events. The various burst detection pipelines are described below.

- Mean filter
  Mean Filter (MF) searches for an excess in a moving average computed on whitened data. Ten different analysis windows, with duration varying from

0.5 ms up to 10ms have been used.

- Power filter
  Power filter (PF) searches on whitened data for a power excess using differ-
  ent time analysis windows and different frequency bands chosen such that
  the product of the frequency and the time duration remain constant [21].In
  the time-frequency plane the PF statistics are derived by taking the loga-
  rithm of the spectrogram.
- Wavelet Detection Filter
  Wavelet Detection Filter (WDF) searches for excess power in a wavelet map
  obtained with a bank of discrete wavelet transforms applied to whitened
  data. A thresholding operation is applied on the wavelet coefficients, and
  only the ones with the largest values are retained. These large coefficients
  are supposed to be linked to the transient signals that exceed the noise
  background [2].
- Peak Correlator
  Peak Correlator (PC) is a matched filter using Gaussian waveform tem-
  plates. The Gaussian templates have been chosen such that the minimum
  match is better than 99% for Gaussian peaks whose σ is between 0.2ms and
  6ms (8 templates???)
- Exponential Gaussian Correlator
  The complex Exponential Gaussian Correlator (EGC) produces a time-
  frequency representation of the data by applying the correlation relation
  for a list of templates of the same family:

$$\Phi_{f_0,Q_0}(t) = exp-2(\pi f_0/Q_0)^2 t^2 \exp 2\pi i f_0 t \tag{2}$$

with (f_0, Q_0) the central frequency and quality factor of the template.

5.2. *Detection of hardware injected signals*

The burst pipelines were tested for the detection of the burst-like signals which
were hardware injected during both runs. Two kinds of signals were injected: Cosine
Gaussian Waveforms and Gaussian Waveform (only during C7 run). We report, as
an example, the results obtained by Power Filter during the C6 run, and the results
by WDF during C7 run. All the burst pipelines run off-line on the data for the
period encompassing the injected events. Fig. 8 shows the distribution of events
found by PF during the C6 run. In the same figure, in blue and red, are displayed
respectively the coalescing binary and burst events detected by the filter during
one of our hardware injection periods. Moreover during C6-run the PF produced
evidence of a set of events that happened regularly every 4 sec. Fig. 9 provides the
the frequency content of these events, and the distribution with respect to the time
distance between consecutive events. We realized that these events were due to the
movements (for alignment) of quadrants used on the optical bench, which produced
mechanical noise that then entered into the dark fringe signal.

10

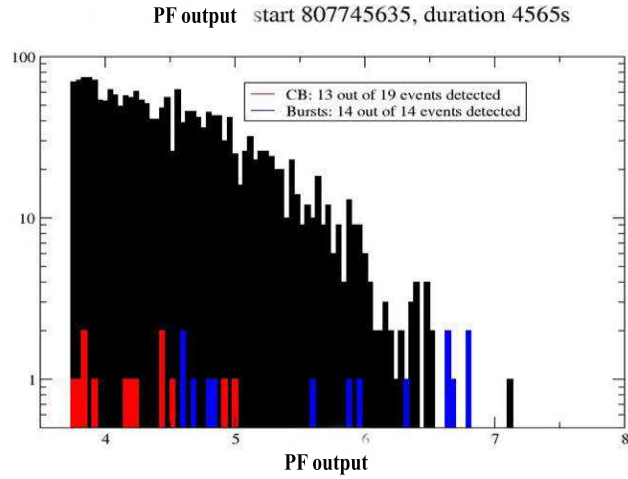**PF output**   start 807745635, duration 4565s

Fig. 8.   Power Filter results on the C6 data during one hardware injection period. The event distribution shows that the data is very noisy. The coalescing binary and burst events are inside the core of event distribution. In red are the coalescing binary events, and in blue are the burst events.
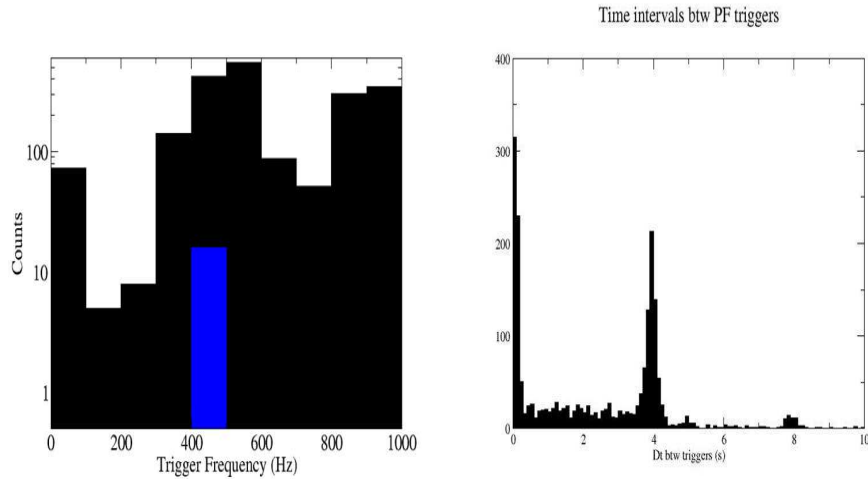

Fig. 9.   Power Filter application. The left plot shows the frequency content of the events found by the power filter. In blue is reported the frequency content for burst detected events, which fit the right injected frequency. The right plot shows the distribution of the events found with respect to the time distance between consecutive events. It is evident that there is a peak at 4 secs, which is the time delay between the movements of the quadrants used during C6.

In Fig. 10 we present, as an example, the results obtained by WDF on the first of the two injection periods during the C7 run. Both the burst and the coalescing binary signals were detected. The coalescing binary detection by a burst algorithm was due to a problem with the hardware injections. The waveforms used for the hardware injections included a sharp end for the inspiral signal, and the subsequent amplitude discontinuity created a wide band excitation; this was detected by our burst search algorithms.
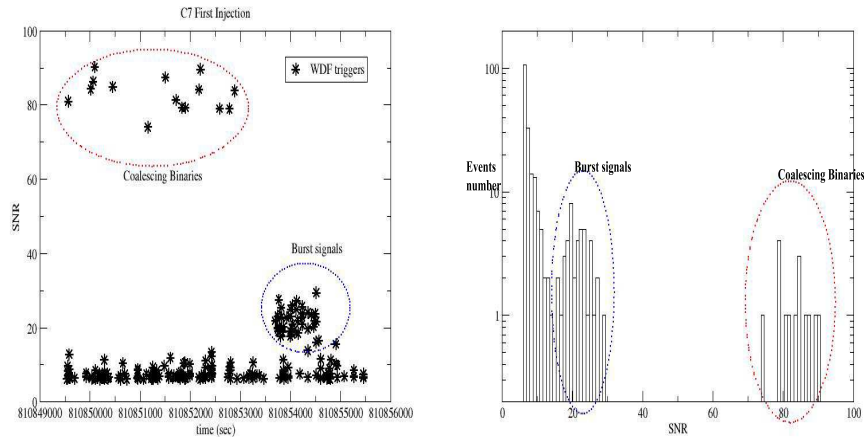

Fig. 10.   WDF detections for the first injection period. The left plot shows the SNR of events with respect to time. The right plot displays the event distribution. The coalescing binary events have been detected with very high SNR because of the problem of the sharp cut-off of these inspiral hardware injections.

5.3. *Veto analysis*

The C6 data was very glitchy as many events were due to the movements of the quadrants for alignment. This created difficulties for the burst analysis. The problem was corrected before the C7 run. As part of the analysis of the C7 data a veto strategy for the cleaning of the event distribution has been established. We tried to identify the channels that can be used as vetoes. Among those channels selected from all of the channels analyzed was a channel that monitors the seismic activity in the mode cleaner building, and another seismic channel that monitors the noise in the detection lab. Fig. 11 presents the events found by the WDF for these two channels. These events were characterized by high values of SNR.

Fig. 12 gives an example of the study of the veto use percentage, that is the percentage of veto triggers that are used to kill events found in the dark fringe inside a given time window, with respect to the SNR threshold for this channel. A
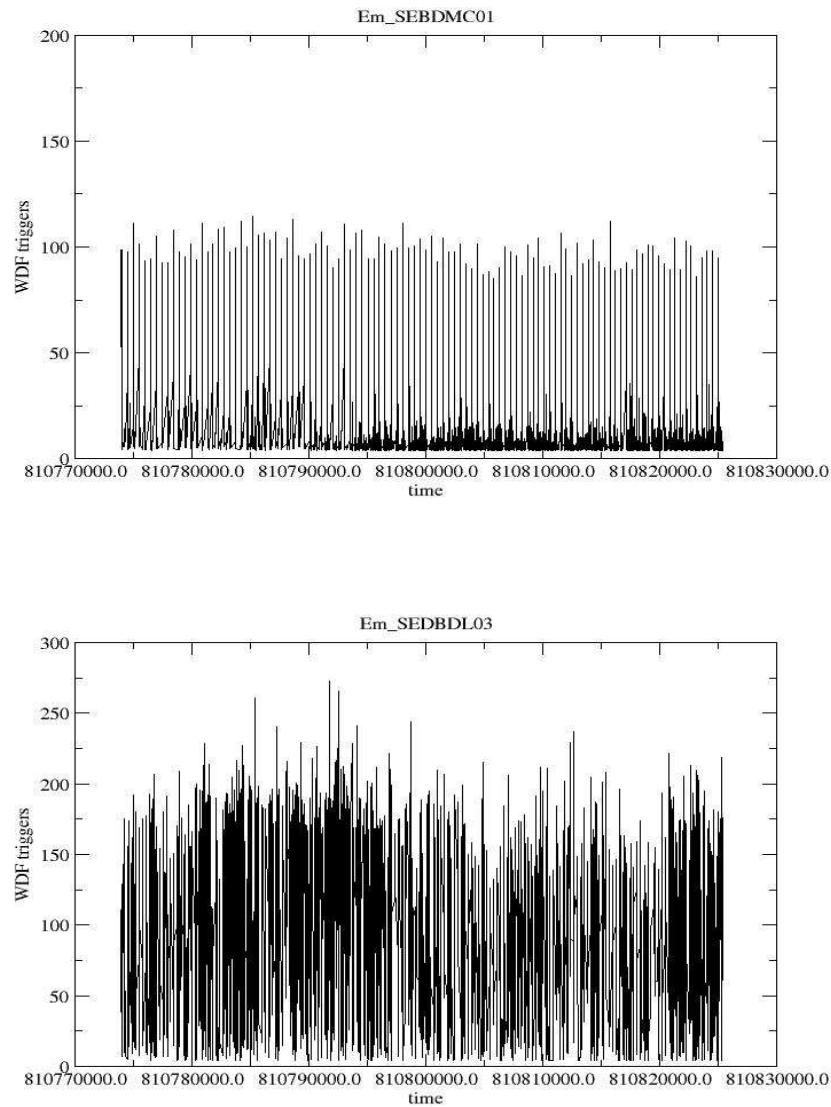
12

Fig. 11.   Events detected by the WDF, as a function of time, for the mode cleaner building and detection lab seismometers. The Mode cleaner are due to the switch on and off of air conditioning system, that's why they are regularly sampled.

plot of this type can help one to select which values to use for the SNR threshold for the events found in the veto channel, and the time veto window to use in order to eliminate coincident dark fringe events. This process cleans the dark fringe event
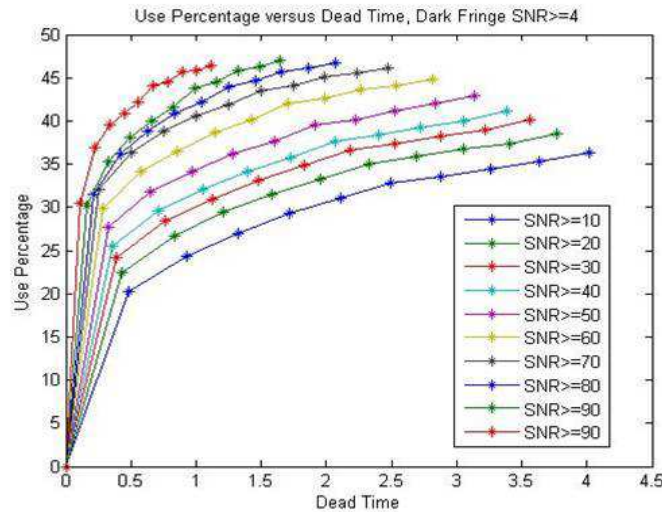
distribution of these noise events.

Fig. 12.   An example of the study of the use percentage for events found with the detection lab seismometer, with respect to the SNR threshold for this veto channel, and also the coincident time window.

5.4. *Burst of bursts (BOB) events*

During the C6 and C7 runs we identified a class of transient events that spoil the data for the burst detection pipelines. These events were characterized by a time duration ranging from 0.5sec to $2 - 3$ seconds; they occur often in the data. We defined these events as burst of burst (BOB) events. It seems that these events are due to the coupling of the frequency noise to the residual motion of a mirror after the alignment control. Fig. 13 shows the behavior of such an event; this data is in the time domain after the whitening procedure (top) and in the time-frequency map (bottom). Different strategies were used to try to clean the data of events due to a BOB. All these methods were linked to channels that monitor the residual motion in the angular degree of freedom of the mirror, or to the laser frequency noise distribution. The frequency noise was monitored with a 1111Hz line injected at laser level, and sidebands due to the coupling with the residual angular motion of the mirror were identified. By monitoring the excess of rms noise around this line, it is possible to identify the presence of a BOB in the data. Fig. 14 shows how the elimination of veto events changes the MF distribution of burst events; the vetoes include the BOB events, and also events in coincidence with triggers in the analyzed seismometer channels. Few high SNR events still survive; we identify the remaining two large SNR events as due to an airplane flying nearby.
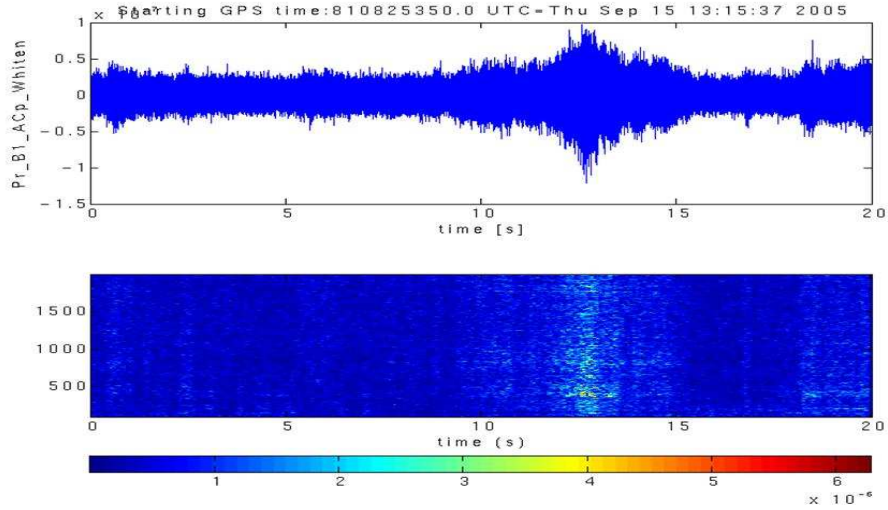
14

Fig. 13.   An example of a BOB event in time domain (top) and in time-frequency domain (bottom). This is from whitened dark fringe signal.
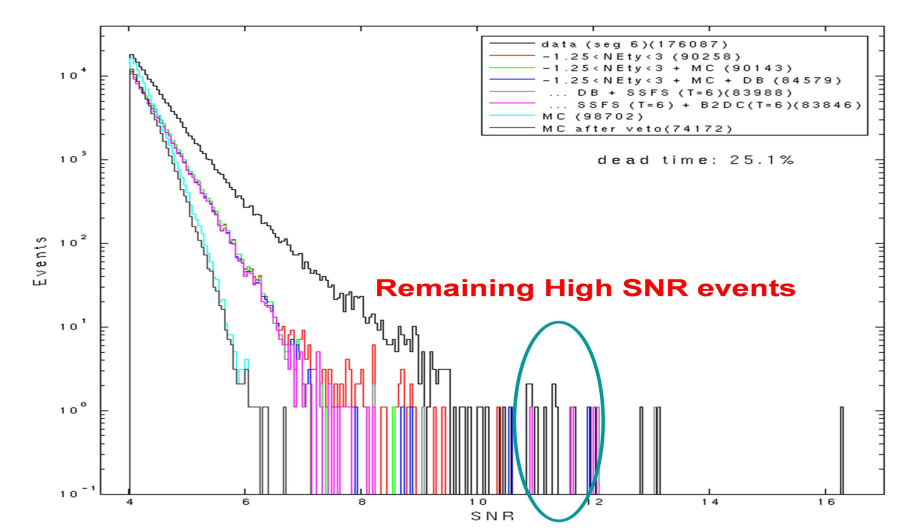
Fig. 14.   Burst event distribution detected by MF after the removal of the events generated by the seismic events in the mode cleaner building and the detection lab, and also the BOB events. Few high SNR events still survive. We identify them as due to an airplane flying nearby.

6. Coalescing Binaries

In Virgo we have two pipelines running for the detection of signals generated by coalescing binary events, specifically the multi-band template analysis MBTA [8], and Merlino [9], which is a parallel implementation based on a message passing

interface (MPI) of standard matched filter techniques. Both the pipelines receive the $h-$reconstructed channel resampled at 4 kHz. The MBTA method is based on splitting the range of frequencies into several bands, searching for events independently in each and recombining the results in a coherent way. Merlino implements a distributed matched filter, based on an MPI. The advantage for MBTA is obtained from a computational point of view, since the different bands can be analyzed at different sampling frequencies. The recombination of results from the various bands can be done in different ways; in exact form it corresponds exactly to the implementation of the matched-filtering procedure. The noise power spectral density (PSD) used by MBTA in the matched filtering is estimated with a frequency resolution of 0.488281Hz, which corresponds to a time window of 2.048s, that is 8192 samples at a 4kHz sampling rate. The PSD is estimated using the classical windowed periodogram method, and in order to follow noise variations two levels of adaptivity are implemented; a running average of the spectral density is computed. Merlino is a signal analysis system designed to efficiently distribute the computation over a cluster running a message passing interface. It is based on a combination of processes that implement different analysis steps:

- a "loader" process receives h-reconstructed data either from the on-line or from a storage system, and applies common pre-conditioning transformations. The most important is the δ filtering, or "double whitening" operation [10], which is the application of a matched filter for δ functions. In the frequency domain, this step corresponds to the transformation $\tilde{h}_{dw}(f) = \frac{\tilde{h}(f)}{S_n(f)}$, with $S_n(f)$ being the noise spectral density, and therefore really implements one of the ingredients of the matched filtering, namely the inverse weighting by the noise spectral density.
- A "group manager" process receives δ-filtered $h_{dw}(t)$ data from the "loader", distributes them to different "worker" processes, each implementing the correlation with templates, and receives back candidate events, which are then clustered[a] and sent down the data acquisition chain[b].
- Each "worker" manages a sub-set of the analysis grid, applying matched filters, and the computationally expensive calculation of the χ^2 veto [11].

The analysis done by the two pipelines was performed over the same parameter space. In particular the range of the masses was $[0.9, 3]M_{\bigodot}$, the frequency range $80Hz - 2kHz$ and the mass grid had a 98% minimal match. Fig. 15 displays the event rate obtained by MBTA during the two runs, focusing on last (best) C6 portion and C7. It is evident that there is a significant non-stationarity in the event rate; this is

---

[a]The clusterization algorithm is very simple; we retain as event parameters, from the entire bank, only those corresponding to the template which issues the largest SNR in a time window of about 0.1s. It does not yet take into account the correlation between different matched filters.
[b]By keeping separate the "group manager" and the loader it will be possible to have separate managers for different searches (binary neutron stars, black holes, . . .)

16

due to the non stationarity of the noise and to the presence of transient-like events, namely the BOB described in section 5.
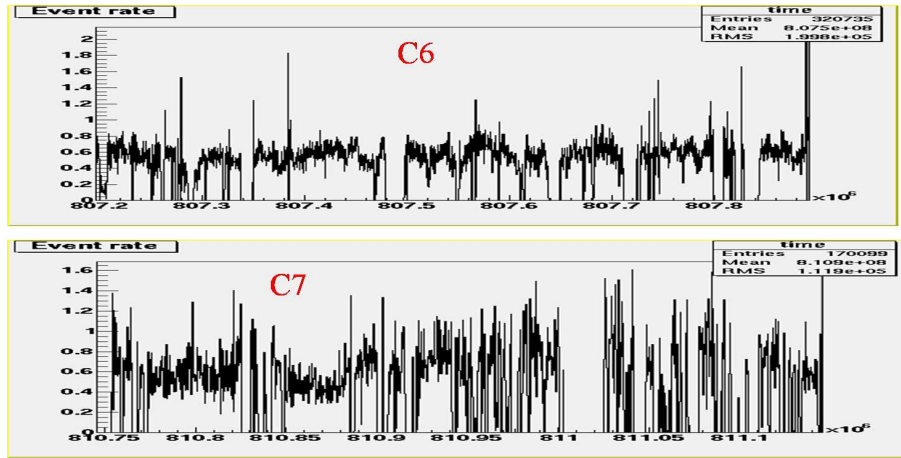

Fig. 15.   Event rates for the MBTA coalescing binary pipeline in C6 and C7

6.1. *Detection of hardware injected signals*

The MBTA or Merlino pipelines both ran on line during C6 and C7. It was possible to immediately see on a web page the results of a trigger, with also the value of χ^2 associated with the events. Fig. 16 shows two typical plots for the events found by Merlino. In the left plot are the values for the masses of the coalescing binary events found by Merlino in the grid distribution. In the right plot are the χ^2 values estimated over 15 bands. It is evident that the events from the hardware injected signals are well separated from the core of the events due to noise. Fig. 17 presents the results obtained by MBTA for the accuracy in the end time and the chirp mass of the injected events. The results are similar for Merlino. Both pipelines were able to detect the injections and obtain very good accuracy for the signal parameters.

6.2. *MCMC*

Parameter estimation, and the generation of a posterior probability density function (PDF) for each parameter, was also done utilizing a Bayesian Markov chain Monte Carlo (MCMC) routine. The basic operation of the inspiral MCMC code is described in [27], which also contains a description of MCMC techniques. The purpose of this code is to take triggers generated from a coalescing binary detection pipeline, and then examine that section of the data about the trigger. The MCMC code was applied to C7 hardware injection signals as a means of ensuring that the injections were not distorted either by the injection or reconstruction procedures.
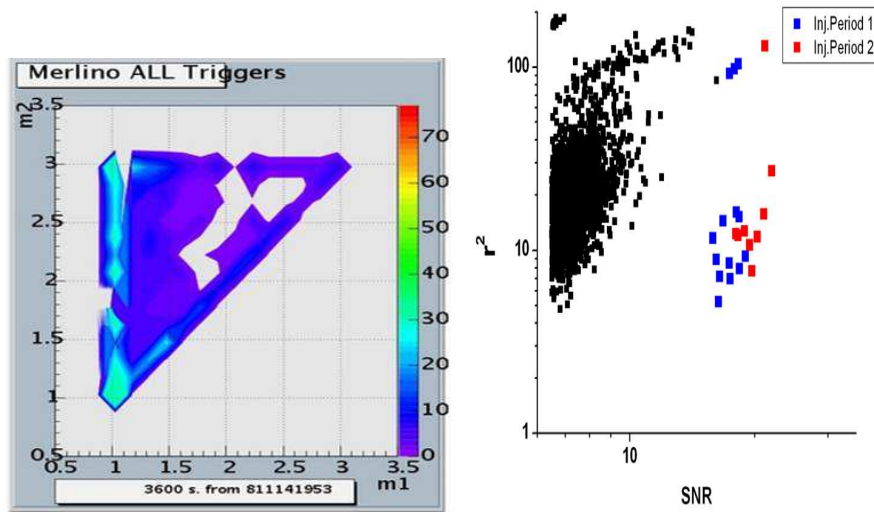
Fig. 16.   Using Merlino triggers, the left plot shows the mass parameter distribution for the detected events for C7 run. The right displays the χ^2 values for the detected events; the blue squares are hardware injections made during injection period 1, while the red squares correspond to period 2.
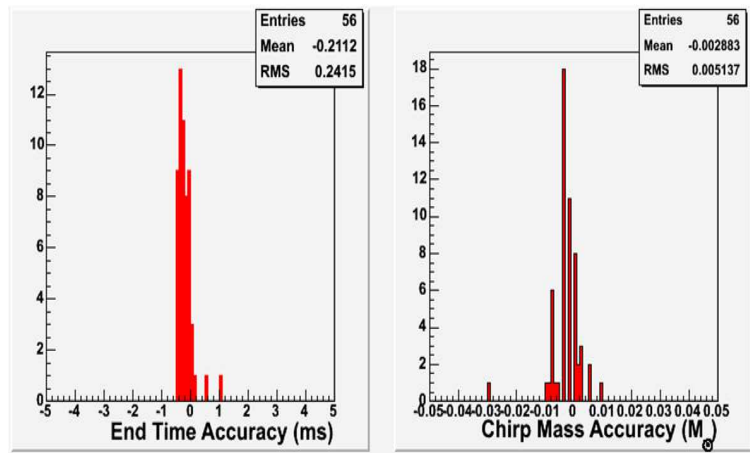

Fig. 17.   End time and chirp mass accuracy from the MBTA pipeline for the hardware injection events during C7-run.

The MCMC searches for events that have a binary coalescence end time within a ±50 ms window (which is the coalescence time prior distribution) of triggers from a coalescing binary search pipeline. The MCMC code looks for inspiral signals based on 2.0 post-Newtonian (PN) signals in the frequency domain. For the C7 application the *prior* for the masses of the compact objects was uniform from 0.9 $M_\odot$ to 3.1 $M_\odot$ range. For this problem there are five parameters to estimate: the

18

binary masses, m_1 and m_2, the effective distance d_L, the phase at coalescence ϕ_c and the time at coalescence t_c. The program reparameterizes the masses in terms of the chirp mass $m_c = (m_1 m_2)^{3/5}/(m_1 + m_2)^{1/5}$ and the mass ratio parameter $\eta = m_1 m_2/(m_1 + m_2)^2$.

The C7 coalescing binary injections simulated signals created with parameter values $m_1 = 1.32 M_\odot$, $m_2 = 1.36 M_\odot$ (giving $m_c = 1.166 M_\odot$ and $\eta = 0.2499$), $d_L = 0.315$ Mpc, and $\phi_c = 1.775$. An example of the MCMC output for one signal can be found in Fig. 18, where the posterior PDFs for the parameters are displayed. From these distributions one can also calculate statistics, such as mean values and 95% confidence intervals. For this particular C7 injection example (at $t_c = 66.6487$) the results were:

parameter	mean	median	95%central posterior interval
m_c	1.1662523	1.1662839	$[1.1656798, 1.1666033]$
η	0.2485865	0.2491488	$[0.2443448, 0.2499979]$
t_c	66.6498213	66.6498250	$[66.6497240, 66.6498949]$
ϕ_c	2.8721900	2.7982841	$[2.5120689, 3.6136382]$
d_L	0.3264991	0.3259644	$[0.3057134, 0.3496863]$

In Fig. 18 the "real" parameter values are at the locations given by the dashed line. All of the parameters are successfully recovered except for a 1 ms offset in t_c; this is due to the fact that the injection signals are created to 2.0 PN in the time domain, but the MCMC's 2.0 PN stationary phase frequency domain detection templates are not their exact Fourier transform.

6.3. *Veto Analysis*

Even if the coalescing binaries group could use the information linked to the knowledge of the theoretical waveforms of the signal, a veto analysis for the understanding of the kind of events that could help in the cleaning the distribution of detected events has been started. In particular, during the C6 and C7 analysis the transient signals due to the saturation of signal used to control the *Second Stage Frequency Stabilization* of the laser, and also power dips in the optical cavity, have been analyzed. Fig. 19 displays an example of a power dip, together with the results of the cleaning of the event distribution due to the implementation of this veto. A more refined separation is possible using the χ^2. In Fig. 16, obtained using Merlino events, we show the scatter plot of the SNR versus the χ^2 value; from this one can see that the events associated with coalescing binary hardware injections have relative low χ^2 values. The χ^2 test was performed using 15 bands, a value found effective in other searches [19].

Another type of veto is one based on the time-domain behavior of the matched filter output [20,21]. In particular, we tested the Shawhan-Ochsner veto using the
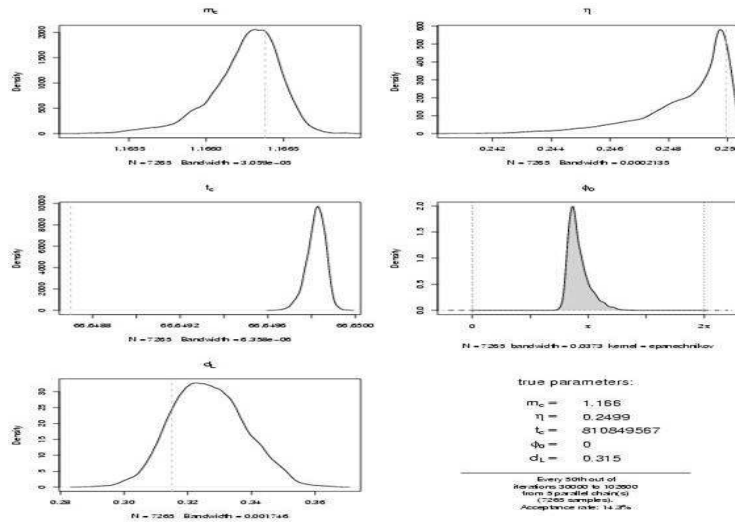
Fig. 18.   Application of MCMC method on C7 Hardware injections, and the resulting posterior PDFs for the parameters.
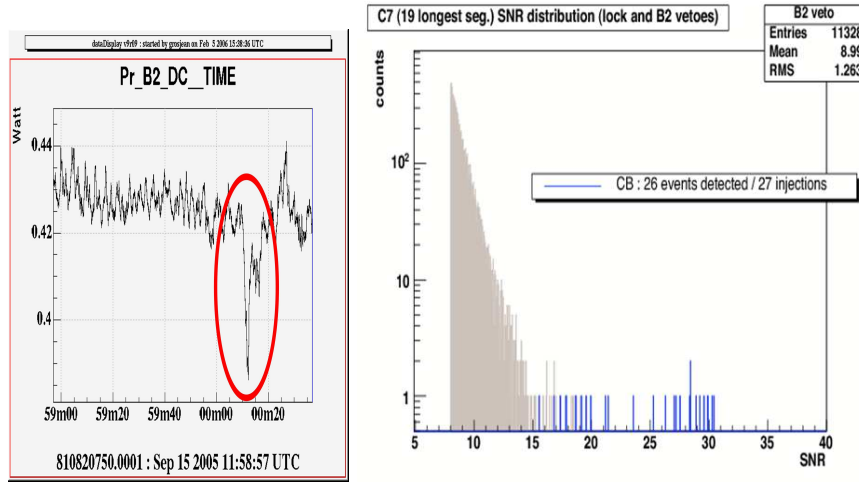

Fig. 19.   A dip in the signal monitoring the power cavity in the power recycling cavity (left), and the results on the dark fringe event distribution after the removal of these type of events.

same settings adopted in [20], namely events are rejected when they pass a threshold λ more than three times before the peak of the event; $\lambda = \sqrt{6.5^2 + SNR^2/6^2}$ is roughly proportional to the SNR of the event. We show in Fig. 20 the results of χ^2 over two bands, and the application of the Shawhan-Ochsner veto on the population of false alarms and also events associated with coalescing binary injections.
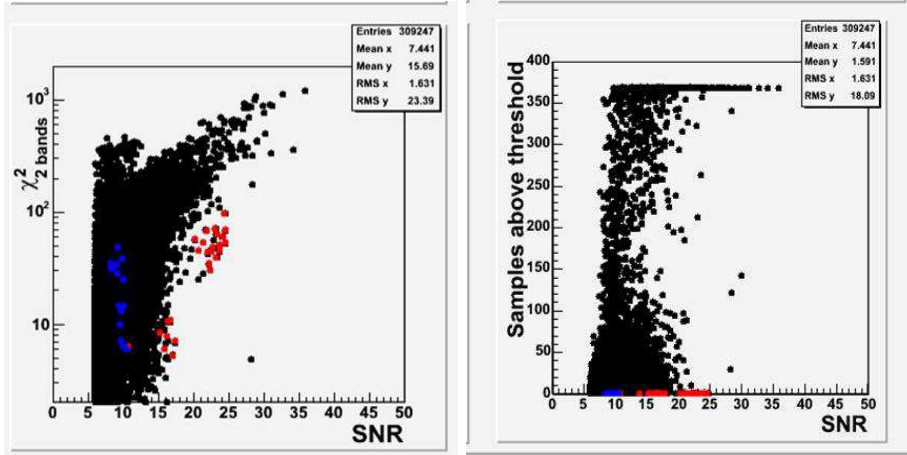
20

Fig. 20.   Using MBTA triggers, the left plot the displays distribution of χ^2 values over two bands with respect to the SNR. The right plot shows the application of the Shawhan-Ochsner veto [20] to the detected events; the red and blue dots correspond to the hardware injections for different injection periods.

7. Stochastic Background

A gaussian, stationary and isotropic stochastic background of gravitational waves is completely described by the cross correlation between the signals $h_A(t)$ coupled to a given detector $\mathcal{D}^A$. This can be written in the frequency domain as

$$\left\langle \tilde{h}_A(f)^* \tilde{h}_B(f') \right\rangle = \frac{1}{2}\delta\left(f - f'\right)\gamma_{AB}(f)\,S_h(f) \tag{3}$$

and can be evaluated knowing the background's power spectrum S_h, together with the positions and the orientations of the instruments involved (this determines the overlap reduction function γ_{AB}). The cross correlation between the outputs of $\mathcal{D}^A$ and $\mathcal{D}^B$ has the structure

$$\langle \tilde{s}_A(f)^* \tilde{s}_B(f') \rangle = \frac{1}{2}\delta\left(f - f'\right)\left[\delta_{AB}S_{n,A}(f) + \gamma_{AB}(f)\,S_h(f)\right] \tag{4}$$

where $S_{n,A}$ is the power spectrum of the noise on $\mathcal{D}^A$, assumed here to be stationary and uncorrelated between the different instruments. In principle it is possible to obtain information about S_h using a single detector, if its noise is fully characterized. This is not the case and probably it never will be, so it is mandatory (and in any case much more efficient) to use several instruments for the detection procedure, obtaining an optimal statistic which can be written as [23]

$$Y_{AB} \propto \int s_A(f)^* \frac{\gamma_{AB}(f)\Omega_{GW}(f)}{f^3 S_{n,A}(f)S_{n,B}(f)} s_B(f)\, df \tag{5}$$

where

$$\Omega_{GW}(f) = \frac{4\pi^2}{3H_0^2}f^3 S_h(f) \tag{6}$$

is a dimensionless quantity proportional to the spectral distribution of the gravitational waves' energy density (see for example [24]). The SNR connected to Y_{AB} can be written as

$$SNR_{AB}^4 \propto T \int df \; \frac{\gamma_{AB}^2(f)\Omega_{GW}^2(f)}{f^6 S_{n,A}(f)S_{n,B}(f)} \qquad (7)$$

where T is the length of the measurement. From this expression it is clear that a low γ^{AB} and an high S_n reduces the contribution of a given frequency interval to the detection efficiency. Using the previous expressions we discuss the collaboration between Virgo and Italian resonant bars using the $C6$ and $C7$ data.

7.1. *Virgo and bars: generalities*

The collaboration between Virgo and Italian resonant bars involves four detectors: the Virgo interferometer, and the Auriga, Explorer and Nautilus resonant bars. The project is mainly a methodological data analysis experiment aimed at the study of detection procedures for a gaussian, isotropic and stationary stochastic background. As discussed in the following we performed injections of simulated signals, initially in simulated noise streams, and then in real data (which for Virgo are the C6 and C7 data sets). Data segments are not synchronized, and for resonant bars they were chosen to be in "quiet" periods. Inside each data set a channel corresponding to the reconstructed strain is provided, together with a minimal quality channel consisting of a boolean flag for each value of the reconstructed strain time series. This flag is used to specify if the corresponding value can be used for the detection or not, for reasons that need not be specified by each member of the collaboration.
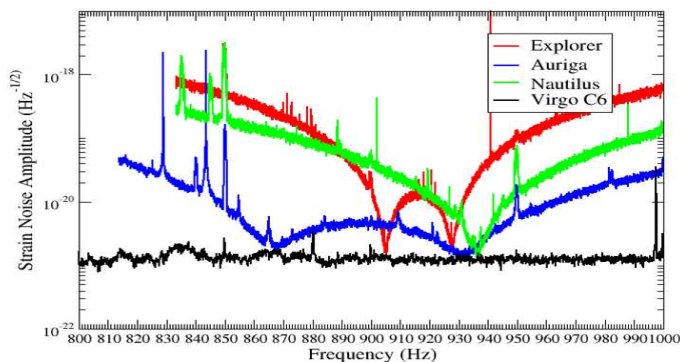

Fig. 21.   Comparison between the sensitivity of the Italian resonant bars and Virgo during the C6 run. The sensitivity is given as an equivalent strain noise amplitude, which is the square root of the S_n single side power spectrum. Sensitivity was estimated from real data.

The main difference between Virgo and resonant bar detectors is the bandwidth,

22

which for a resonant bar is of the order of few tens of Hz. At the frequencies
which correspond to its detection band the sensitivity of a resonant bar is currently
comparable with the one achieved in Virgo during the C6 run, as can be seen from
Fig. 21. We see that the common detection band is in the range $850 - 950$ Hz.

As the SNR is limited by the noise power spectra (that appears in the denom-
inator of Eq. (7)) it follows that the contribution of Virgo will be limited also to
the bars' detection band. To show this in a more quantitative way we can plot the
integrand in Eq.(7) as a function of the frequency, as displayed in Fig. 22¸ using
four months of data and current sensitivities (the C6 one for Virgo). Apparently
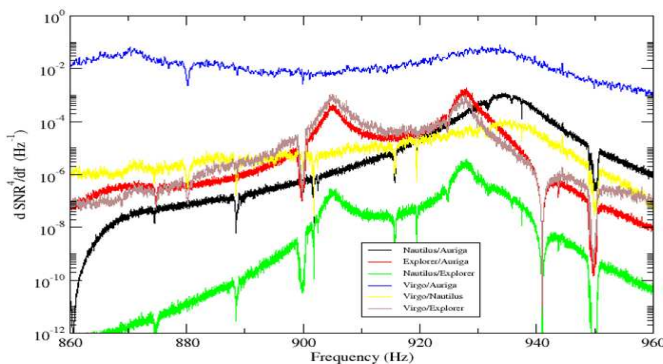the largest contribution to sensitivity is the one of the Virgo/Auriga pair.

Fig. 22.   The integrand of Eq. (7) as a function of the frequency, for each pair of detector involved
in the Virgo/bars collaboration.

From Eq. (5) we see that the optimal correlation statistic depends on the back-
ground's power spectrum through the factor Ω_{GW}. The injected signal was chosen
to be limited to a frequency independent Ω_{GW}, but owing to the small bandwidth
this is not expected to be a very relevant factor. The quantity SNR^4 is additive, so
it is possible to define a SNR for the entire network which is simply connected to
the upper bound for the stochastic background amplitude achievable. Namely, the
smaller detectable Ω_{GW} is proportional to SNR^{-2}, the proportionality factor be-
ing dependent on the desired false alarm and detection rates. Inserting the present
sensitivities we find that an upper limit for $h_{100}^2\Omega_{GW}$ (in some units) is achievable.
If we project this result on the final sensitivities foreseen for the different detectors
we find that we could obtain $h_{100}^2\Omega_{GW} < 10^{-2}$.

7.2. *Simulation and detection pipeline*

The software used for both the simulation and the detection of the stochastic back-
ground signal was implemented by the Virgo stochastic background group. It is built

on the top of a general purpose data analysis library written in C++ (NAP) [26] as a specialized C++ library with python bindings. The final simulation and detection pipeline is implemented as a python script which can be easily modified and configured.

The simulation algorithm allows for the generation of an arbitrary number of time series with the correct cross correlation properties defined by Eq. (3). In order to do that the square root $K_{AB}(f)$ of the cross correlation array is evaluated using a standard factorization algorithm in the frequency domain, $\gamma_{AB}S_h = K_{AC}K_{CB}$. The array $K_{AB}(f)$ is the frequency domain representation of a filter which must be applied to a vector of uncorrelated white noise to obtain the final result. In order to avoid boundary effects on the filtered data, which could be a time series of arbitrary large length, a standard overlap and add procedure is applied.

To check the correctness of the simulation procedure we can easily estimate S_h from each of the detectors' channels. It is also easy to see that the coherence between the channels, which correspond to detectors $\mathcal{D}^A$ and $\mathcal{D}^B$, is simply the overlap reduction function γ_{AB}. As an example we compare in Fig. 23 the theoretical squared overlap reduction function with the one estimated from the simulated data, in the frequency domain relevant for the project.
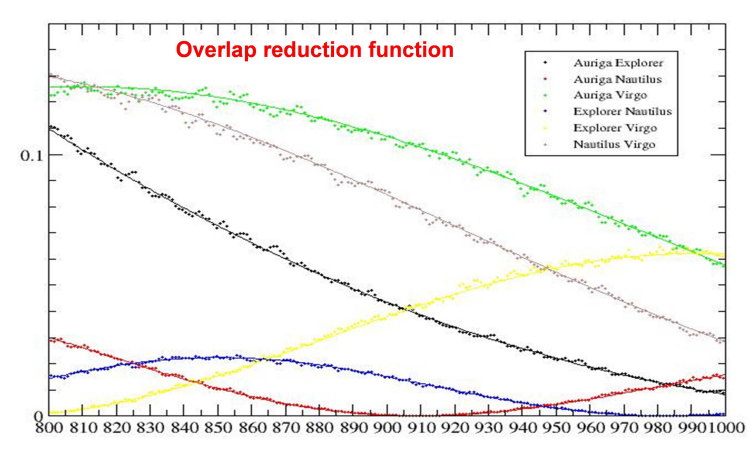

Fig. 23.   The theoretical squared overlap reduction function γ^2_{AB} for each pair of detectors involved in the project (continuous lines) compared with the squared coherence between the corresponding simulated data streams.

The main technical complication in the implementation of the detection pipeline is connected to the fact that resonant bars' data were provided in an heterodyned form. We choose to apply the same transformation to the Virgo data, in order to save space and computational time. The steps used to obtain this are summarized in Fig. 24. Starting from the C6 data we apply first of all a band pass filter to eliminate the frequency component outside the common frequency band of the collaboration.

24

Next, the data are heterodyned, and a low pass filter is applied to eliminate the spurious higher frequency components generated. The last step is the decimation of the data, which are resampled at the same rate as that of Auriga. The Explorer and Nautilus data are provided at a different sampling, and are also adjusted.
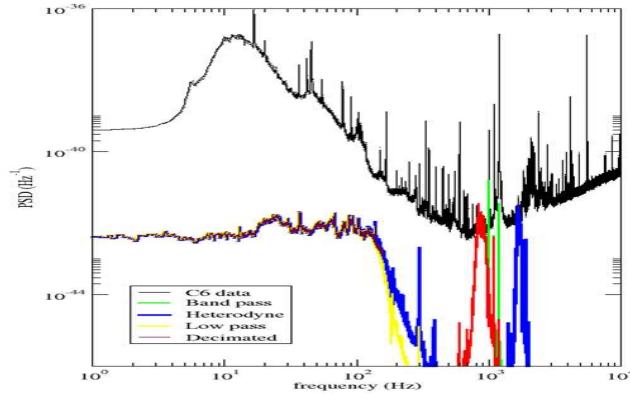

Fig. 24.   Spectral amplitudes of the C6 data after the application of each step of the conversion to the appropriate heterodyned format. The black plot correspond to the original data, the green one to the data after the application of a band pass filter which preserve them only in the detection band of the resonant bars. After the heterodyning this green peak is split in two copies at high and low (around zero) frequency, plotted in blue. A low pass filter preserve only the low frequency region (yellow) and the data are finally resampled (brown).

The statistical analysis of the results initially was focused on characterization of the noise. The real detection procedure consists in the estimation of the optimal correlator Y^{AB} together with their theoretical variance after the injection of signals at SNR of 1, 2, 5 and 10. This analysis is currently in progress.

In the future moreover, the possibility to exchange real data with the Ligo Scientific Collaboration will extend this activity to the full Virgo sensitivity band, making our activity even more promising.

7.3. *A results concerning C6 noise.*

The detection pipeline is a good test bed for a real detector noise, which can fail to satisfy the standard assumptions of stationarity and gaussianity. We present here the results of the analysis of stationarity obtained during the study of the preprocessing stage. The stationarity of the noise is an important assumption for the application of the standard detection strategy. Several estimates of the optimal correlator Y_{AB} obtained from short stretches of data can be averaged together in a simple way only if their standard deviation is constant. If this is not true appropriate weighting and vetoing procedures should be implemented. For this reason we concentrated from the start on the detection of non stationary data.
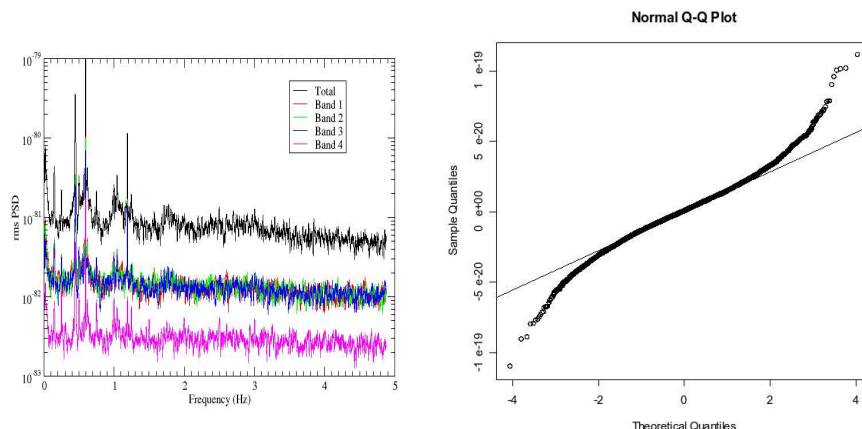
Fig. 25.   On the left, the power spectral density of a time series containing the energy in the detection band $850 - 950\,Hz$ estimated over short time periods (in black). The other curves represent the same quantity estimated in the sub bands $850 - 875\,Hz$, $875 - 900\,Hz$, $900 - 925\,Hz$ and $925 - 950\,Hz$. On the right, the quantile-quantile plot for the distribution of the data in the same band.

A standard time-frequency analysis applied on the detection band gave negative results. As a second step we studied the frequency distribution of the signal power. In Fig. 25 we plot the power spectrum of the time series constructed with the energy contained in consecutive short time stretches. It shows at least three clear peaks at $f = 0.446, 0.594, 1.190\,Hz$ ($T = 2.24, 1.683, 0.84\,s$) which indicate a quasi periodic oscillation of the general noise level. This conclusion is indirectly confirmed by the study of the distribution of the data $s(t_i)$ inside the detection band. For stationary noise this is expected to be a gaussian distribution with squared width proportional to the rms. But looking at the quantile-quantile plot in Fig. 25 we see clearly that the distribution has tails larger than the expected. The interpretation is that the (gaussian) distribution of data has a time dependent width, so that the cumulative distribution is no more a gaussian one.

Typically the stretch of data used to estimate the optimal correlator Y_{AB} is of the order of some tens of seconds, which is large compared with the typical oscillation periods observed. For this reason we expect that this kind of non stationarity should not have a big impact on the detection efficiency. On the other hand this effect should be further studied, and in our opinion is an example of the utility of a feedback between data analysis and commissioning groups.

8. Conclusion

We have reported on the analysis done by the Virgo data analysis physics groups on the data acquired during the two runs C6/C7 done by the Virgo experiment during 2005. The data were not at a good sensitivity to do a scientific study, but were long and stable enough to test the detection pipelines and setup strategy for

26

the cleaning of the results after a better comprehension of the noise distribution was achieved. Veto strategies were put in place by burst and coalescing binary groups. The analysis results gave important feedback to the commissioning group in order to help solve hardware problems in the interferometer that could make the noise distribution dirty with fake events. For example, we observed the movements of the quadrants on the optical bench and the coupling of frequency noise with residual motions of the mirrors, which caused the BOB events.

Moreover, the analysis of simulated noise is an important first step for the validation of algorithms and software, because the gaussianity and stationarity properties are assured for the optimal detection pipelines.

The use of real data allows for the testing of veto procedures and the definition of data quality indicators. As the Virgo noise is rapidly evolving some of these indicators will not be useful at the design sensitivity, but can give, in any case, information that is very useful for noise hunting and commissioning.

References

1. C. Bradaschia and et al (Virgo collaboration), *Nucl.Instrum.Methods* **289**, 518 (1990).
2. E. Cuoco, *VIR-NOT-EGO-1390-308* **internal note** (2005).
3. Bradaschia C et al. (the Virgo collaboration) 1990 *Nuclear Instruments and Methods* **289**, 518-525.
4. Braccini S et al. (the Virgo collaboration) 2005 Status of Virgo, these proceedings.
5. Veziant O et al. (the Virgo collaboration) 2003 *Class. Quant. Grav.* **20**, S711
6. Beauville F 2005 Prélude à l'analyse des données du détecteur Virgo: De l'étalonnage à la recherche de coalescences binaires Université de Savoie PhD Thesis
7. Flaminio R 2000 Int.J.Mod.Phys. **D**, 9-3.
8. F Marion *et al.* 2003 Multi-band search of coalescing binaries applied to Virgo CITF data, Proceedings of the "Rencontres de Moriond".
9. Amico P, Bosi L, Cattuto C, Gammaitoni L, Marchesoni F, Punturo M, Travasso F, Vocca H 2003 *Comp. Phys. Comm.* **153**, 179.
10. Cuoco E et al. 2004 *Class.Quant.Grav.* 21, S801-S806.
11. Allen B 2005 *Phys. Rev.*D **71** 062001 (*Preprint* gr-qc/0405045).
12. Bosi L, Buskulic D, Cella G, Cokelaer T, Guidi G M, Viceré A 2004 The inspiral library user manual.
13. Beauville F, Buskulic D, Flaminio R, Marion F, Massonet L, Mours B, Ramonet J, Tournefier E, Veziant O and Yvert M 2003 *Class. Quant. Grav.* **20**, S789.
14. Buskulic D 2005 Placement of templates in parameter space using interpolated iso-match ellipses on a triangulated grid, *Preprint* gr-qc/0504046.
15. Blanchet L, Iyer B R, Will C M and Wiseman A G 1996 *Class. Quantum Grav.* **13**, 575.
16. Bosi L, Brocco L, Beauville F, Guidi G M and Viceré A 2005 Hardware injections of signals during the C5 run, *Preprint* VIR-NOT-FIR-1390-291
17. Dimmelmeier H, Font J A, Müller E, 2002 *Astron. Astrophys.* **393** 523-542.
18. Beauville F, Bosi L B, Buskulic D, Guidi G M, Marion F, Mours B, Viceré A, 2005 Search for inspiralling binaries signals in Virgo C5 data, *Preprint* VIR-NOT-FIR-1390-301.
19. Abbott B et al. (LSC) 2005 *Phys. Rev.*D **72**, 082001.
20. Shawhan P, Ochsner E 2004 *Class. Quant. Grav.* **21**, S1757-S1765.

21. Guidi G M 2004 *Class. Quant. Grav.* **21**, S1767-S1774.
22. Acernese F et al. (the Virgo collaboration) 2005 *Class. Quantum Grav.* **22**, S1139-S1148.
23. B. Allen and J. Romano, 1999 Phys. Rev. D **59** 102001.
24. M. Maggiore, Phys.Rept. 331 (2000) 283-367
25. I. Fiori et al Virgo Internal Note (2006).
26. E. Cuoco for Virgo Collaboartion, CQG (2005) S1041
27. C. Roever, R. Meyer, N. Christensen, Classical and Quantum Gravity, Vol. 23, p. 4895 (2006).
28. same proceedings.